DEFENCE R&D DÉFENSE

An Analysis of RADARSAT2 SAR-GMTI Performance for Standard Beam Mode

Shen Chiu
Defence Research Establishment Ottawa

Defence R&D Canada

DEFENCE RESEARCH ESTABLISHMENT OTTAWA

TECHNICAL REPORT
DREO TR 2000-088
December 2000

National Defence Défense nationale

Canada

DEFENCE R&D DÉFENSE

An Analysis of RADARSAT2 SAR-GMTI Performance for Standard Beam Mode

Shen Chiu
Space Systems Group
Space Systems and Technology Section

DEFENCE RESEARCH ESTABLISHMENT OTTAWA

TECHNICAL REPORT
DREO TR 2000-088
December 2000

Project
5EG11

Abstract

Canada's RADARSAT2 (R2) commercial SAR satellite will have an experimental operating mode that will allow ground moving target indication (GMTI) measurements to be made with received data. This mode is also called MODEX (Moving Object Detection Experiment). In the GMTI or MODEX mode of operation, the spacecraft's radar antenna is partitioned into two apertures that sequentially observe the scene of interest from the same points in space. Data is simultaneously and coherently received from both apertures and is down-linked in parallel channels for processing to extract moving target radial speeds in their SAR image context. This paper provides an analysis of SAR-GMTI performance at the R2 Standard Beam Mode based on computer modeling and simulations. Two SAR-MTI processing approaches are being explored. One utilizes the classical DPCA clutter cancellation technique to provide sub-clutter visibility for dim slowly moving targets. The other is based on the along-track (temporal) SAR interferometer technique, where amplitude and phase information of the slow-moving targets are exploited to allow their extraction from the dominant clutter background. Performances of the two approaches are compared. Effects of target signal contamination by background clutter is also examined. The results indicate that the two processing approaches are similar in their GMTI performance.

Résumé

Le satellite RAS commercial RADARSAT2 (R2) du Canada sera doté d'un mode expérimental qui permettra d'effectuer des mesures en vue de l'indication de cibles terrestres mobiles (GMTI), à partir des données reçues. Ce mode est appelé mode GMTI ou MODEX (expérience de détection d'objets mobiles). En mode GMTI ou MODEX, l'antenne radar de l'engin spatial est divisée en deux ouvertures qui observent successivement la scène d'intérêt à partir des mêmes points de l'espace. Les données sont reçues simultanément et de façon cohérente des deux ouvertures et sont transmises par liaison descendante dans des canaux parallèles pour fins de traitement en vue d'extraire les vitesses radiales des cibles mobiles dans leur contexte d'image RAS. Le présent article renferme une analyse des performances du RAS-GMTI en mode de faisceau standard du R2, basée sur la modélisation et des simulations informatisées. Deux méthodes de traitement des données du RAS-MTI sont examinées. L'une fait appel à la technique classique de suppression du clutter par DPCA pour produire la visibilité dans les échos parasites de cibles floues se déplaçant lentement. L'autre fonctionne selon les principes du RAS interférométrique longitudinal (temporel), où l'information d'amplitude et de phase des cibles mobiles se déplaçant lentement est utilisée pour les extraire du clutter de fond dominant. Les performances des deux méthodes sont comparées. On examine également les effets de la contamination du signal de cible par le clutter de fond.

Executive summary

Canada's RADARSAT2 (R2) satellite will have an experimental operating mode, called R2 MODEX (Moving Object Detection Experiment), which will allow ground moving target indication (GMTI) measurements to be made.

This paper reports on an investigation of the GMTI performance of two SAR-GMTI processors, currently being developed for R2 MODEX, based on computer modeling and simulations. One utilizes the classical DPCA clutter cancellation technique to provide sub-clutter visibility for dim slowly moving targets. The other is based on along-track (temporal) interferometric SAR principles, where amplitude and phase information of the moving targets are exploited to allow their extraction from the dominant clutter background.

The proposed R2 "dual-receive" mode uses the full antenna on transmit, while the antenna is divided into fore and aft apertures on receive. An "alternating-transmit" mode has also been considered, where pulses would be alternately transmitted from each sub-aperture of the antenna. Only the "dual-receive" mode was considered in this study. Realistic radar GMTI signals were generated using a sophisticated space-based MTI radar simulator known as the SBRMTISIM. In this paper, only one of R2's beams, known as a Standard Beam Mode, was examined to predict the R2 GMTI performance.

The GMTI signal was generated based on 20 targets with ground speeds ranging from 3 to 15 m/s and RCS from 20 to 45 m^2, moving within land clutter with a reflectivity of −10 dB m^2/m^2 and Rayleigh distributed amplitudes. Five simulation runs with exactly the same scenario but different random number generation seeds were conducted. The results indicate that the two processing approaches are similar in their GMTI performance. The SAR/DPCA has an average of 12.6 detections and 7.0 false alarms, and the SAR/ATI has about the same detection value, 12.4, with 7.8 false alarms.

Comparison of the two processors indicates that the SAR/DPCA suffers the shortcoming of its processed signal voltage being dependent on the target radial velocity. Thus, significant target signal reduction, due to DPCA-filter modulation, occurs at low radial speeds. On the other hand, the SAR/ATI output is the signal power and its magnitude is not a function of the target radial speed. However, due to target signal contamination by background clutter, the apparent SAR/ATI phase angle of the target is consistently lower than the actual value. This effect is most severe for small signal-to-clutter-ratio targets, rendering their detection more difficult.

Target signal contamination by background clutter was also examined. The result clearly shows that clutter contamination from the moving target's pre-shifted position is negligible and that the contamination comes mainly from the SAR-shifted position.

The initial simulation results are encouraging and suggest that detection of ground moving targets of sufficient RCS is possible with a sensor of the RADARSAT2 GMTI class.

Chiu, S. 2000. An Analysis of RADARSAT2 SAR-GMTI Performance for Standard Beam Mode. DREO TR 2000-088. Defence Research Establishment Ottawa.

Sommaire

Le satellite RADARSAT2 (R2) du Canada sera doté d'un mode expérimental, appelé MODEX (expérience de détection d'objets mobiles), qui permettra d'effectuer des mesures en vue de l'indication de cibles terrestres mobiles (GMTI), à partir des données reçues.

Le présent article fait rapport d'une enquête sur les performances GMTI de deux processeurs RAS-GMTI, en cours de développement pour le MODEX du R2, basée sur la modélisation et des simulations informatisées. L'un fait appel à la technique classique de suppression du clutter par DPCA pour assurer la visibilité dans les échos parasites de cibles floues se déplaçant lentement. L'autre fonctionne selon les principes du RAS interférométrique longitudinal (temporel), où l'information d'amplitude et de phase des cibles mobiles est utilisée pour les extraire du clutter de fond dominant.

En émission, le mode MODEX proposé du R2 fait appel à l'ensemble de l'antenne, tandis qu'en réception, l'antenne est divisée en une ouverture avant et une ouverture arrière (mode de « réception double »). On a également envisagé un mode « d'émission alternée » dans lequel les impulsions seraient émises alternativement de chaque ouverture de l'antenne. Seul le mode de « réception double » a fait l'objet de cette étude. Des signaux radar GMTI réalistes ont été générés au moyen d'un simulateur de radar MTI spatial sophistiqué désigné SBRMTISIM. Dans le présent article, un des faisceaux du R2 seulement, connu sous le nom de faisceau standard, a été examiné en vue de prédire les performances GMTI du R2.

Le signal GMTI a été généré en fonction de 20 cibles avec des vitesses au sol allant de 3 à 15 m/s et des SER allant de 20 à 45 m^2, se déplaçant à l'intérieur d'un clutter de sol avec une réflectivité de -10 dB m^2/m^2 et des amplitudes à distribution de Rayleigh. On a effectué cinq essais de simulation avec exactement le même scénario, mais avec des germes différents de génération de nombres aléatoires. Les résultats indiquent que les deux méthodes de traitement sont semblables à l'égard de leurs performances GMTI. Le RAS/DPCA a une moyenne de 12,6 détections et de 7,0 fausses alertes, et le RAS interférométrique accuse à peu près le même nombre de détections, soit 12,4 avec 7,8 fausses alertes.

Une comparaison des deux processeurs indique que le RAS/DPCA présente un inconvénient : la tension de son signal dépend de la vitesse radiale de la cible. Par conséquent, il y a un affaiblissement considérable du signal de cible aux vitesses radiales réduites. Par contre, la sortie du RAS interférométrique correspond à la puissance du signal, et sa valeur n'est pas fonction de la vitesse radiale de la cible. Cependant, à cause de la contamination du signal de cible par le clutter de fond, l'angle de phase apparent de la cible du RAS interférométrique est systématiquement

inférieur à sa valeur réelle. Cet effet est le plus prononcé dans le cas des cibles à SER réduite, ce qui rend leur détection plus difficile.

On a également examiné la contamination du signal de cible par le clutter de fond. Le résultat montre clairement que la contamination par le clutter à partir de la position avant le déphasage de la cible mobile est négligeable et que la contamination est principalement due à la position déphasée par le RAS.

Les résultats initiaux de la simulation sont prometteurs et suggèrent que la détection de cibles terrestres mobiles de SER suffisante soit possible avec un détecteur de classe GMTI du RADARSAT2.

Chiu, S. 2000. An Analysis of RADARSAT2 SAR-GMTI Performance for Standard Beam Mode. DREO TR 2000-088. Le Centre de recherches pour la défense Ottawa.

Table of contents

List of figures

List of tables

Acknowledgements

Special thanks to Dr. Chuck Livingstone and Mr. Tony Knight for their valuable advice and guidance throughout this work and to Georgio Dinardo for his computer support. This work is supported by the DREO Space Systems Group.

1.0 Introduction

A space based radar (SBR), operating at 800 km altitude, has an orbital speed of approximately 7.5 km/s. Under the RADARSAT2 antenna design constraints (this is a synthetic aperture radar satellite), acceptable range and azimuth ambiguity levels can be achieved for the two GMTI apertures using pulse repetition frequencies (PRFs) in the vicinity of 2000 Hz, for terrain grazing angles between 80° and 40°. The radar design allows PRFs up to 3800 Hz to be selected by accepting ambiguity level and swath width trade-offs. The available PRF and grazing angle ranges result in the majority of the received signal spectrum being occupied by strong clutter returns from the "stationary" terrain. Since the radar is fundamentally a SAR, there is no azimuth beam steering capability that would allow the radar beam to dwell on a point on the earth's surface more than the synthetic aperture time. Single channel GMTI measurements, based on the extraction of the target Doppler spectrum are severely constrained to large cross section, rapidly moving, targets whose motion has a large radial component.

The detection probability and the estimation accuracy can be increased considerably by use of multiple aperture antennas. Space-time adaptive processing (STAP) techniques can be used to provide sub-clutter visibility for dim slowly moving targets. The displaced phase center antenna (DPCA) technique, which is a form of STAP, is well suited for SBR. This technique requires at least two antenna phase centers be arranged along the flight direction, each with its own dedicated receiver channel. The phase centers of the two sub-apertures are displaced physically in such a way that a pair of pulses from the two receivers appear to be generated from a stationary radar when an appropriate sampling rate (i.e. PRF) is chosen. Since the clutter Doppler frequency from a stationary radar is concentrated at dc, a conventional MTI canceller can be used to null the background clutter. This is the classical DPCA two phase center clutter suppression technique. In this approach, the received signals from channels 1 and 2 are time shifted to register them spatially, then subtracted to cancel the background clutter. Target enhancement is limited by the noise floor, the phase noise of the radar, the scene phase noise and the target fading.

This paper reports on an investigation of the GMTI performance of two SAR-MTI processors currently being developed for RADARSAT2. The two SAR-MTI processing architectures are introduced in Sec. 2.0. This is followed by a discussion of the newly proposed RADARSAT2 GMTI mode in Sec. 3.0, including its sensor configuration and parameters. Sec. 4.0 looks at the SBRMTISIM simulation tool used to simulate realistic radar signals and Sec. 5.0 defines the experimental scenario to be used for this study. Simulation results are then presented in Sec. 6.0. The two GMTI approaches are then analyzed and compared in Sec. 7.0. Sec. 8.0 examines the effect of target signal contamination by background clutter. Finally, Sec. 9.0 provides some conclusions.

2.0 GMTI Processor Architectures

Three types of MTI processing are being considered for RADARSAT2 MODEX mode: SAR displaced phase center antenna (DPCA) processing, along-track interferometry (ATI), and space-time adaptive processing (STAP). In this investigation we will only consider the first two processors.

The proposed GMTI processors for RADARSAT2 MODEX are shown in Fig. 1. The first MTI processor, which we shall call the SAR/DPCA processor (see Fig. 1a), is the limiting case of the two-beam DPCA clutter canceller. The pulses from the leading antenna are delayed by T, the integral pulse number needed to effectuate the DPCA condition. SAR processing is then performed on each channel. The outputs of the SAR modules are subsequently subtracted to yield a GMTI image. The stationary clutter signals are suppressed, and only signals from moving targets with sufficient radial velocity remain.

In true classical DPCA, target detection would be performed on the raw difference data. Performance may be improved by taking advantage of the SAR capability of the system and performing SAR processing on the difference data prior to detection. Due to theoretically perfect clutter cancellation of DPCA, any remaining targets in the image will correspond to moving targets. Since SAR processing is a linear operation, the SAR processing on the difference data is equivalent to performing SAR processing on the two apertures separately, and then taking their difference. The utilization of the SAR/DPCA technique to provide SAR and MTI simultaneously has been discussed by other authors [1, 2].

In a similar way to classical DPCA, SAR/ATI uses two-displaced phase centers aligned along-track. Instead of taking the difference of the two channels, the interferometric phase is computed. This is done, as in other types of interferometry, by generating SAR images for each channel separately, and then estimating the interferometric phase by computing the phase (i.e., the complex argument) of the product of one image with the complex conjugate of the other (see Fig. 1b). The remaining phase is zero for stationary objects and non-zero otherwise. The application of the SAR/ATI technique to GMTI have also been discussed by other investigators [3, 4].

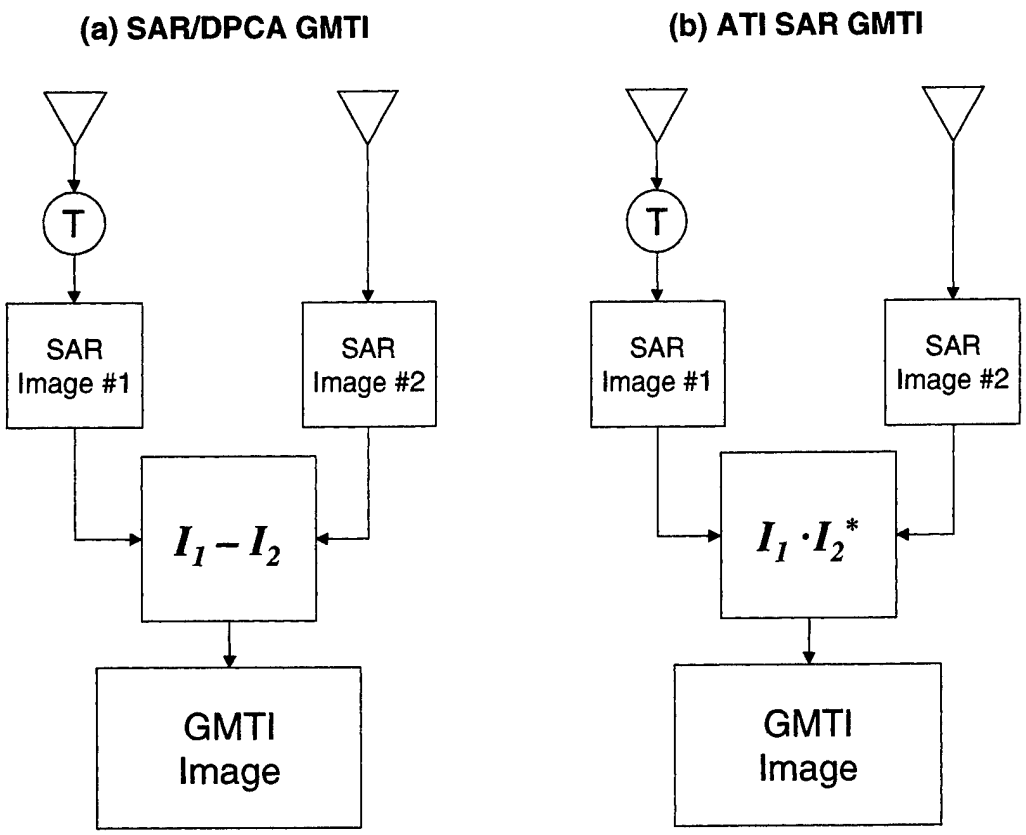

Fig. 1 Two simple SAR-GMTI processor architectures: (a) SAR/DPCA GMTI and (b) SAR/ATI GMTI.

3.0 RADARSAT2 GMTI Mode

At present time, no satellite-borne radar system has a GMTI capability. Although all of the processes needed for full function GMTI have been developed for airborne systems, differences in platform velocity, range to target, and accessible depression angles between airborne and spaceborne radars result in several unknown parameters for the optimization of spaceborne GMTI sensors. Cost, complexity, available technology, and design risk have all combined to preclude the construction and launch of a full-function space-based GMTI radar.

When the detailed properties of GMTI and SAR systems are examined, a restricted set of GMTI functions can be added as operating modes to an appropriately designed SAR with little impact on the radar design. The RADARSAT2 MODEX is thus the world's first attempt to implement such a limited-function GMTI aboard a commercial SAR satellite. Although the subset of possible GMTI operating modes available from a radar of this type is small, such a radar could be used to validate GMTI parameters and algorithms needed for more sophisticated radars.

RADARSAT2 is currently under development and is scheduled for launch in Spring 2003. Preliminary information on the RADARSAT2 MODEX configuration can be found in references [5, 6]. Table 1 lists some of the SAR-MTI sensor characteristics and design parameters.

Table 1: RADARSAT2 SAR-GMTI Parameters

Parameter	Value
Orbit Description:	
Type	Circular
Inclination	98.6°
Altitude	800 km
Active Array:	
Length × Width	15 m × 1.5 m
Number of sub-apertures	2
Orientation	Long-axis forward, Elevation boresight ±29.5° (selectable)
Look Geometry:	
Nominal Incidence Angle	10° to 60°
Search Type	Strip-map
Swath Size	150 km to 25 km
Azimuth Beam Width	Programmable from 0.21° to 0.63°
Detection Cell Size	Programmable from 25m×25m to 3m×3m

Waveform:	
Band	5.405 GHz
Bandwidth	10 to 100 MHz
Peak Power	2.4 kW (42 μs pulse) 3.7 kW (21 μs pulse)
Duty Ratio	10 %
PRF	1300 to 3800 Hz
Burst Length	up to 500 ms
Receiver Noise Temperature:	695 K

Detection cell sizes are based on RADARSAT2's standard beams and the new ultrafine beam that operates at 100 MHz bandwidth to produce 3m×3m image resolution cells. The RADARSAT2 antenna looks broadside to track. While this limits the capability to dwell on an area of interest for theater defence applications, it should be well-suited as an experimental SAR-GMTI sensor, providing very useful real data.

The proposed "dual-receive" mode uses the full antenna on transmit, while the antenna is divided into forward and aft apertures on receive. The one-way phase center separation can be controlled by the number of columns used for receiving, but have a nominal value of 7.5 m. An "alternating-transmit" mode has also been considered, where pulses would be alternately transmitted from each sub-aperture of the antenna. This mode would give a larger two-way phase center separation than the dual-receive mode. However, only the first "dual-receive" mode will be considered in this study.

4.0 SBRMTISIM Simulator

The simulation results described in the next section were obtained using a sophisticated space-based MTI radar simulator known as the SBRMTISIM, developed by Sicom Systems Ltd. for DND. The simulator provides an Environment Window showing a world map overlaid with the satellite ground track. The user can specify the look-geometry and define clutter regions and targets to create a scenario (see Fig. 2). Clutter is modeled as a set of regularly distributed scatterers with user specified cross-section, statistics and internal motion. Targets are modeled as point scatterers with user specified cross-section and fading statistics. Other windows are used to specify the radar and antenna parameters, and other parameters needed to characterize the system. Once these parameters are specified, the simulator generates high-fidelity, complex baseband signals representing the signals received by the SBR. The complete, two-way path of the signal is modeled from the transmitter, to the earth, and back to the receivers.

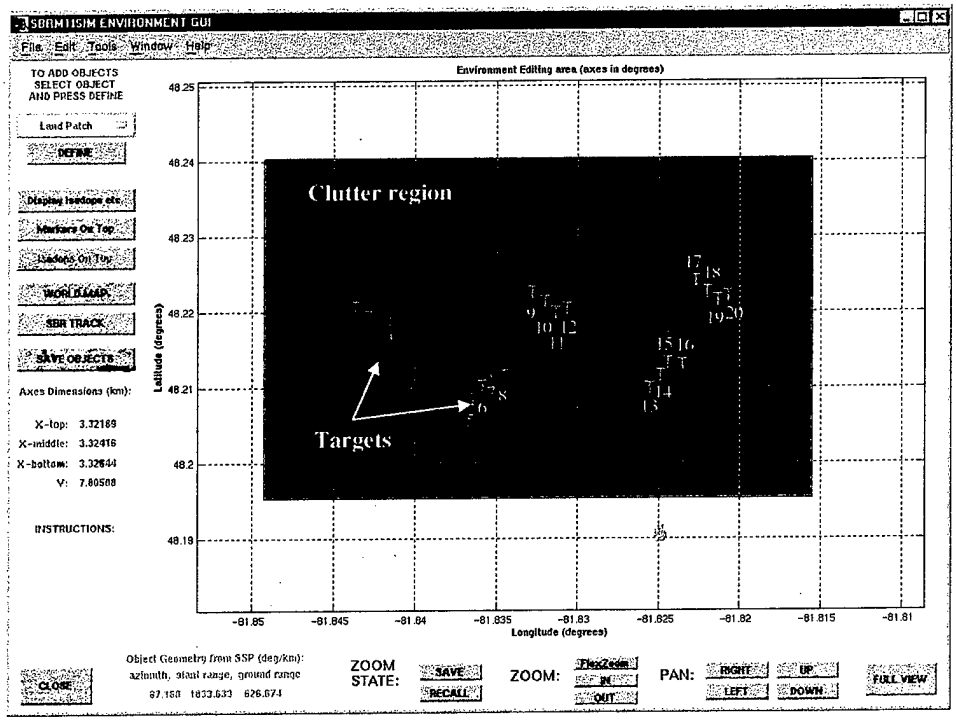

Fig. 2 SBRMTISIM Environment Window

The simulator then passes the generated data to a customized, built-in processing module, in which the architecture and algorithms are specified by the user. One of the processor options is the SAR/DPCA architecture as illustrated in Fig. 1a. The

SAR/ATI processor option (Fig. 1b) has also been implemented, and a constant false-alarm rate (CFAR) detector suitable for the SAR/ATI processed signal output is currently under development. Some preliminary results are presented in Sec. 6.0.

5.0 Experimental Definition

One of RADARSAT2's beams known as a Standard Beam Mode provides swaths in the 120 km to 170 km range with multi-look ground image resolutions of about 25 m × 25 m. This mode is expected to be useful for GMTI surveillance for large strong targets [5]. In this paper, only the standard beam mode is investigated for predicting the GMTI performance of RADARSAT2.

A carefully designed scene is created using the Environment Window (Fig. 2). A range swath of 1500 m was generated, which contains a 2.5 km × 5.0 km land-clutter patch having a reflectivity of –10 dB m^2/m^2 and a spectral width of 0.1 m/s. The clutter amplitudes are Rayleigh distributed. The same target and clutter scenario is used for both SAR/DPCA and SAR/ATI processing architectures.

A total of 20 targets occupy the clutter region (Fig. 2), with key target parameters summarized in Table 2. The targets cover a typical range of radial speeds and target radar cross-sections. The details of the simulation parameters are also listed in Appendix A.

Table 2: Target Parameters

Target Number	RCS (m^2)	Speed (m/s)
1	45	15 (east)
2	45	10 (east)
3	45	5 (east)
4	45	3 (east)
5	40	15 (west)
6	40	10 (west)
7	40	5 (west)
8	40	3 (west)
9	35	15 (east)
10	35	10 (east)
11	35	5 (east)
12	35	3 (east)
13	30	15 (west)
14	30	10 (west)
15	30	5 (west)
16	30	3 (west)
17	20	15 (east)
18	20	10 (east)
19	20	5 (east)
20	20	3 (east)

The satellite heading is approximately north with right-looking geometry. The targets are heading either east or west; as a result, the moving targets have significant radial components toward or away from radar.

A waveform with a PRF of 1988 Hz provides the necessary DPCA condition for clutter cancellation. This PRF generates 750 ms of data for each of the two 7.5 m receive sub-apertures.

6.0 Simulation Results

The first test case is one with 20 moving targets but with both the land clutter and the thermal noise removed from the scene. The generated raw signal data are passed through the SAR/DPCA processor and the targets are detected using a cell-averaging CFAR detector to produce a MTI image as shown in Fig. 3. As expected, the MTI image is very clean with no noise- or clutter-contributed false alarms. All 20 targets are detected irrespective of their RCS or speed. The positions of these targets are shifted in azimuth according to their respective radial speed. The target-only MTI image serves as the reference for the subsequent full scenario simulation.

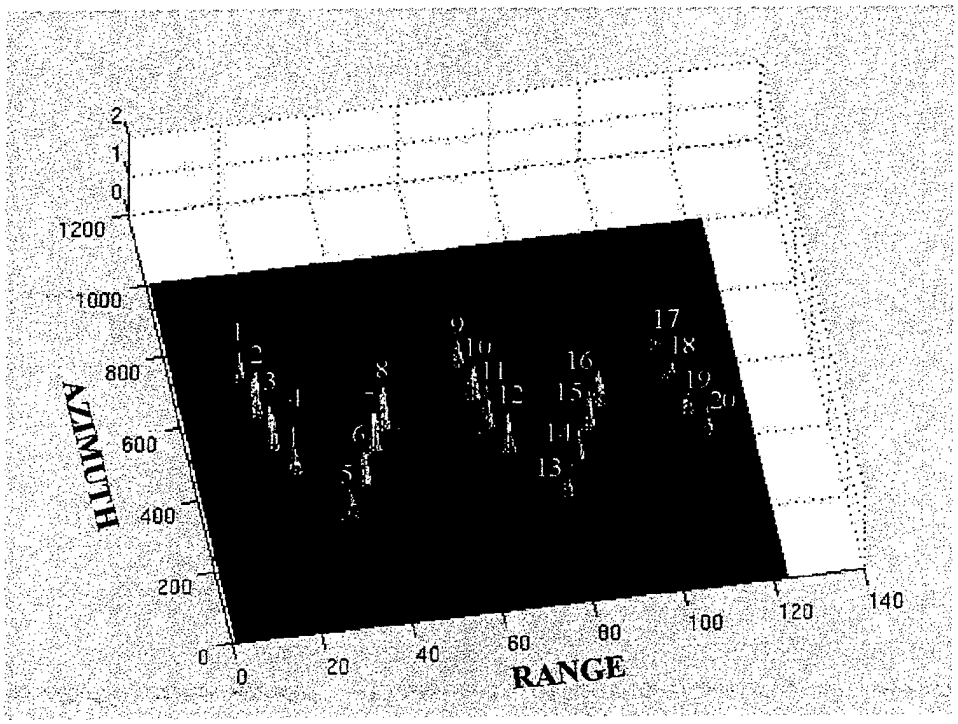

Fig. 3 MTI image of 20 moving targets without the land clutter and the thermal noise.

Next, a full scenario with targets, clutter and thermal noise signals is generated. Each channel's signal data are SAR-processed separately to produce two SAR images. Fig. 4 shows the SAR image from channel 1. Most targets are below the background clutter and no moving targets are detectable. This is expected since the brightest target in the scene has a signal-to-clutter ratio (SCR) of only about 1.2 dB. Plotting the same SAR signal in the complex plane as shown in Fig. 5, one sees that the targets are completely buried in this clutter "noise ball," making the target detection virtually impossible.

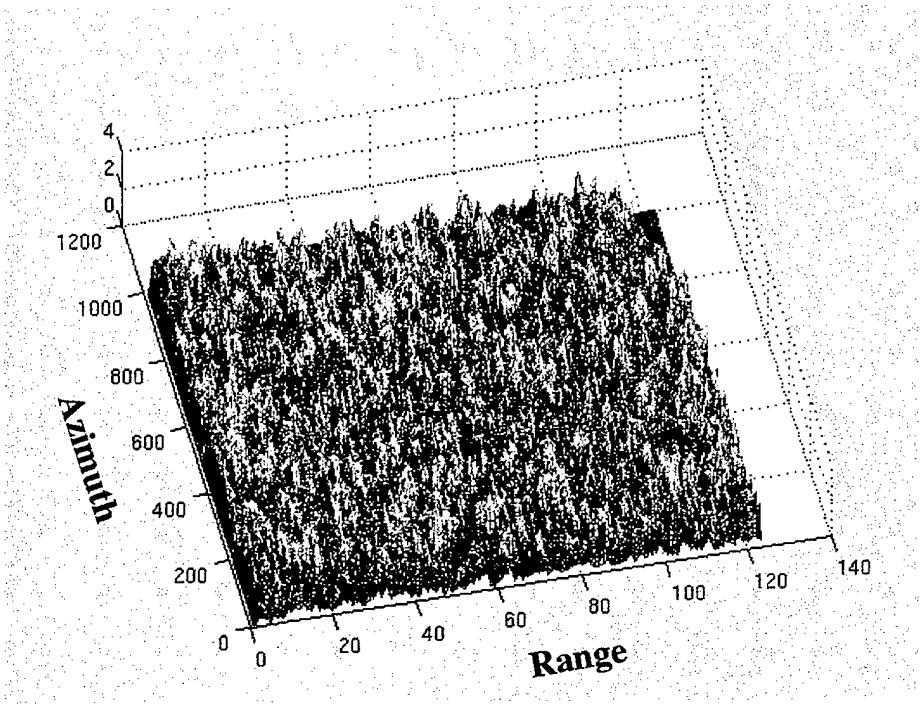

Fig. 4 Signals from channel 1 after SAR processing.

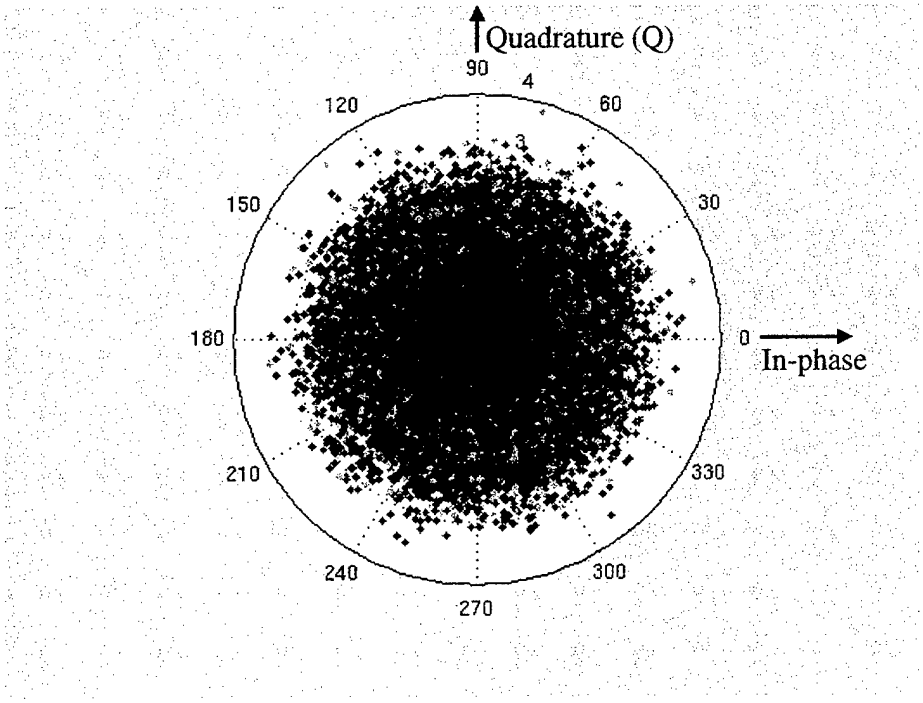

Fig. 5 Complex-plane plot of Channel 1 SAR signal.

Continuing with the signal processing chain, as depicted in Fig. 1a, the SAR signal of channel 1 is time shifted by an inter-pulse period T and then subtracted from channel 2 to produce a MTI image. As can be seen in Fig. 6, the stationary clutter signals are suppressed or whitened, leaving only the signals from the moving targets and the noise floor. The I-Q plot of the SAR/DPCA output signal is also shown in Fig. 7. The coherent clutter signal is clearly suppressed with most of the targets above the noise level.

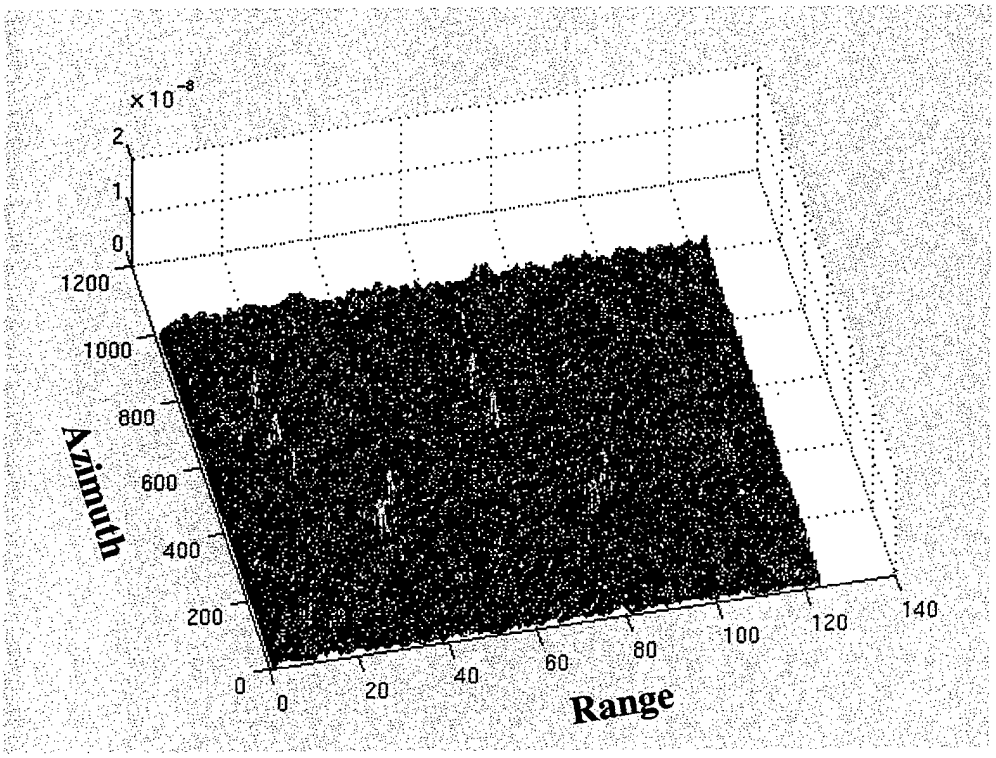

Fig. 6 Output signal from the SAR/DPCA processor, with clutter signal reduced to the noise level and some moving target signals clearly visible.

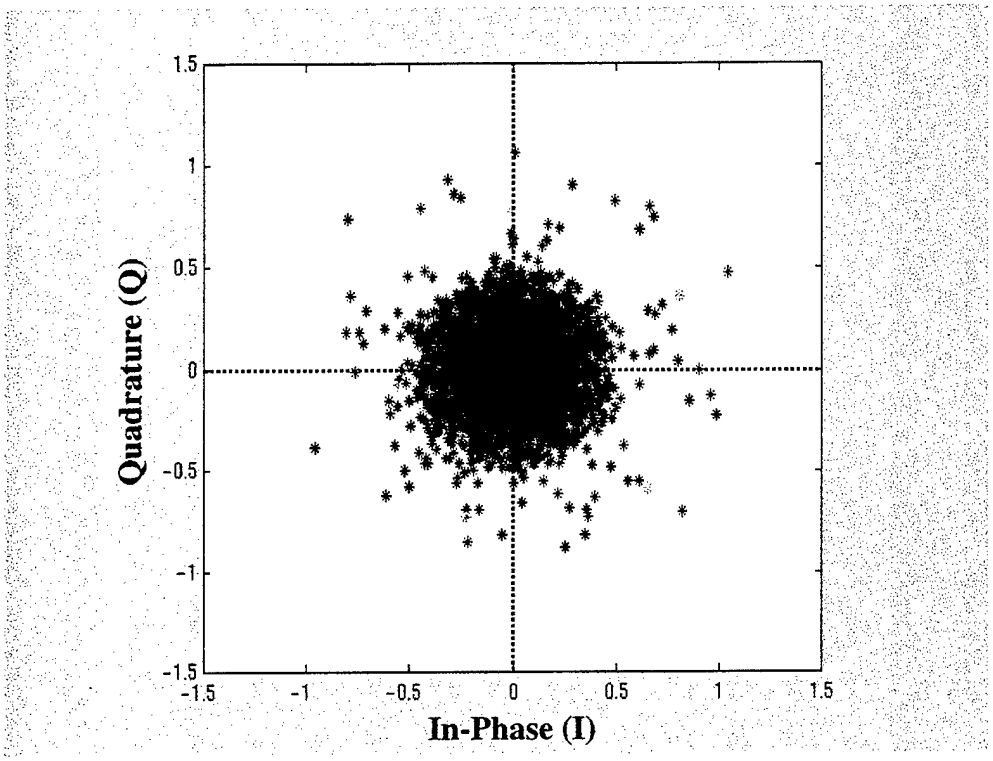

Fig. 7 Complex plane plot of SAR/DPCA output signal. Dots lying outside the noise "ball" are the moving target signals.

Passing the SAR/DPCA signal through a CFAR detector, one obtains a MTI plot as shown in Fig. 8. In this case, almost all of the 15 m/s and 10 m/s targets are detected except for the 20 m^2 RCS target #17. However, all the 3 m/s targets are missed and only two of the five 5 m/s targets are detected. This is expected since the magnitude of the SAR/DPCA output signal or the "difference vector" is of the form $\sin(x/2)$, where x is directly proportional to the target radial velocity. Thus, slow-moving targets are attenuated or suppressed along with the stationary clutter. In this test, three of the four 20 m^2 targets are missed, indicating that long integration times provided by SAR are necessary for dim target detection and that MTI is also needed if reliable detection is to be achieved in clutter.

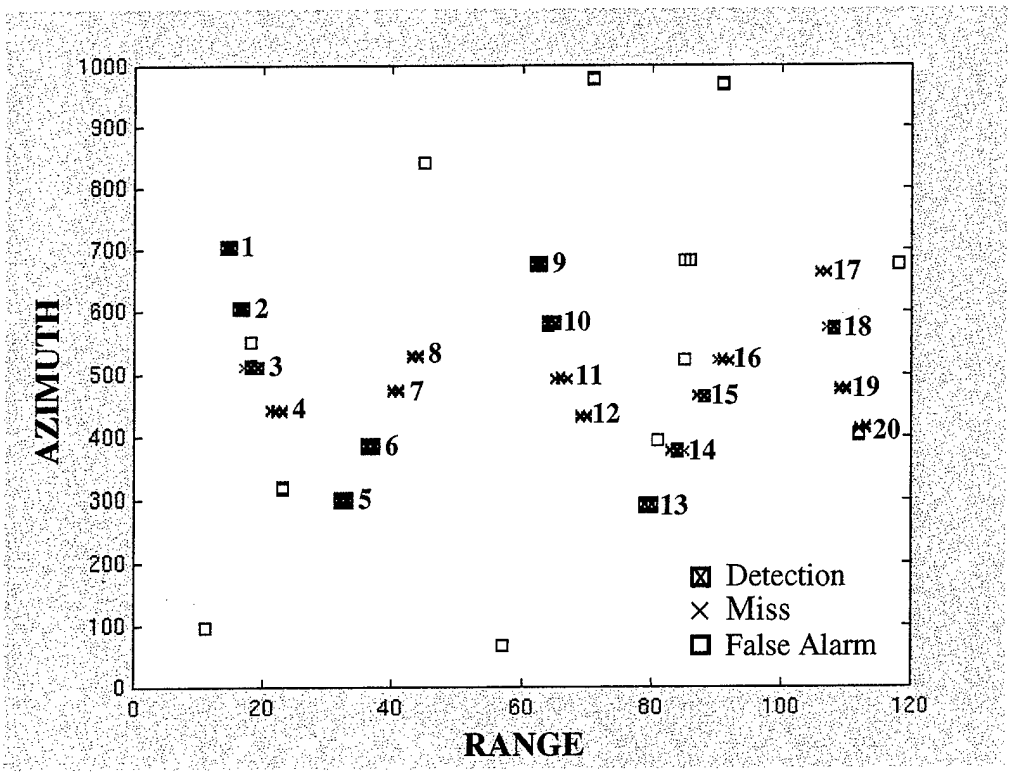

Fig. 8 Output of CFAR detector.

With the SAR/ATI processing architecture (Fig. 1b) the SAR signal from channel 1 is time shifted by an inter-pulse period T and then multiplied with the conjugate of the SAR signal of channel 2 to produce an interferometric SAR image. The I-Q plot of this SAR/ATI image signal is shown in Fig. 9. The clutter-signal phase is "cancelled" giving a mean zero phase. The phase spread of the main lobe clutter around the x-axis (or in-phase axis) is due to the thermal noise, the phase noise, and other noises of the system. Moving targets with finite radial velocities appear in the figure as vectors with non-zero phases. It is clear from the plot that those moving target vectors residing outside the main clutter region can be detected using a suitably devised detection scheme. Here we would like to suggest a simple method based on empirically fitting a set of I-Q points derived from Q-component distributions of the signal data.

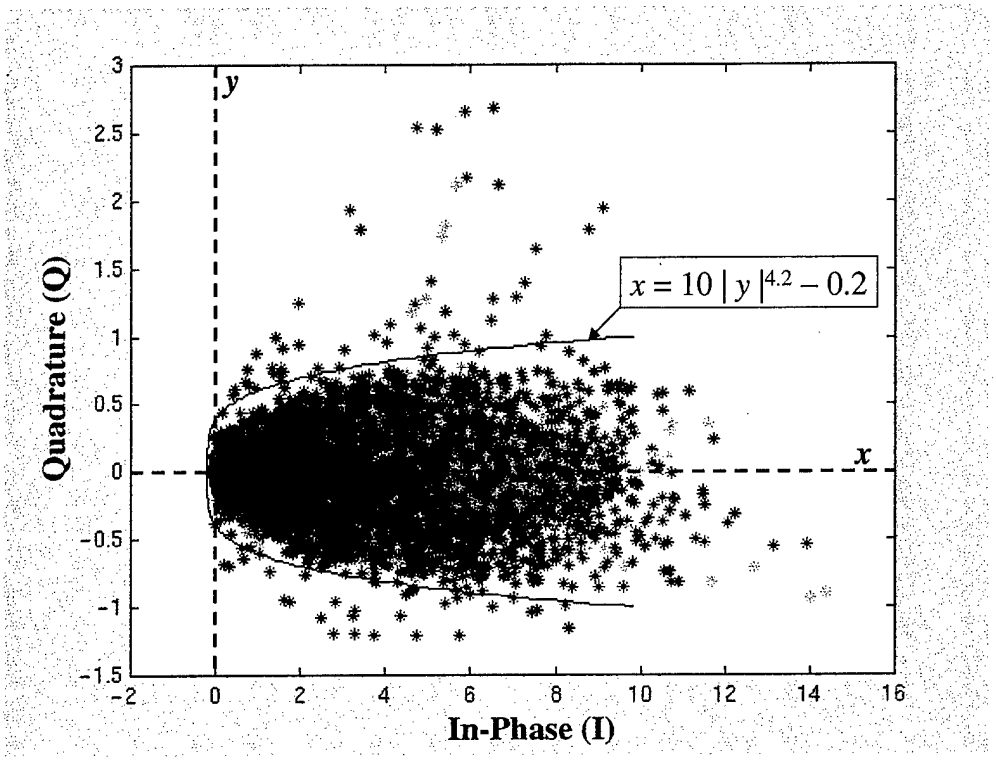

Fig. 9 Output signal from SAR/ATI processor, with clutter phases center around zero and moving target phases at non-zero values.

We proceed by dividing the x-axis into equally spaced segments and then plot the Q-component distribution of each of these segments as shown in Fig. 10. We find that the Q-component of the clutter has a Gaussian distribution. This may be expected since if the thermal noise is dominant noise component contributing to the main lobe clutter scatter and since the thermal noise is normally distributed in magnitude, we would expect also a normally distributed Q-component.

By fitting these normally distributed Q-components with best normal curves and deriving their statistical parameters, we can then calculate the y (or Q-component) values for each of the x segments based on the desired probability of false alarm as follows:

$$P_{FA} = \frac{2 \cdot \int_{y=y_o}^{y=+\infty} e^{-\frac{y^2}{\sigma^2}} dy}{\int_{y=-\infty}^{y=+\infty} e^{-\frac{y^2}{\sigma^2}} dy} .$$

Solving the equation for y_o one then obtains a y-value for a given x segment . The factor 2 in the numerator takes into account the fact that the normal distribution is symmetric. The above procedure yields a set of (x, y) data points to which one can fit a $x = F(y)$ curve. This best-fit curve is the detector that can be used to discriminate the moving targets from the stationary clutter and that will yield the specified false alarm rate P_{FA}.

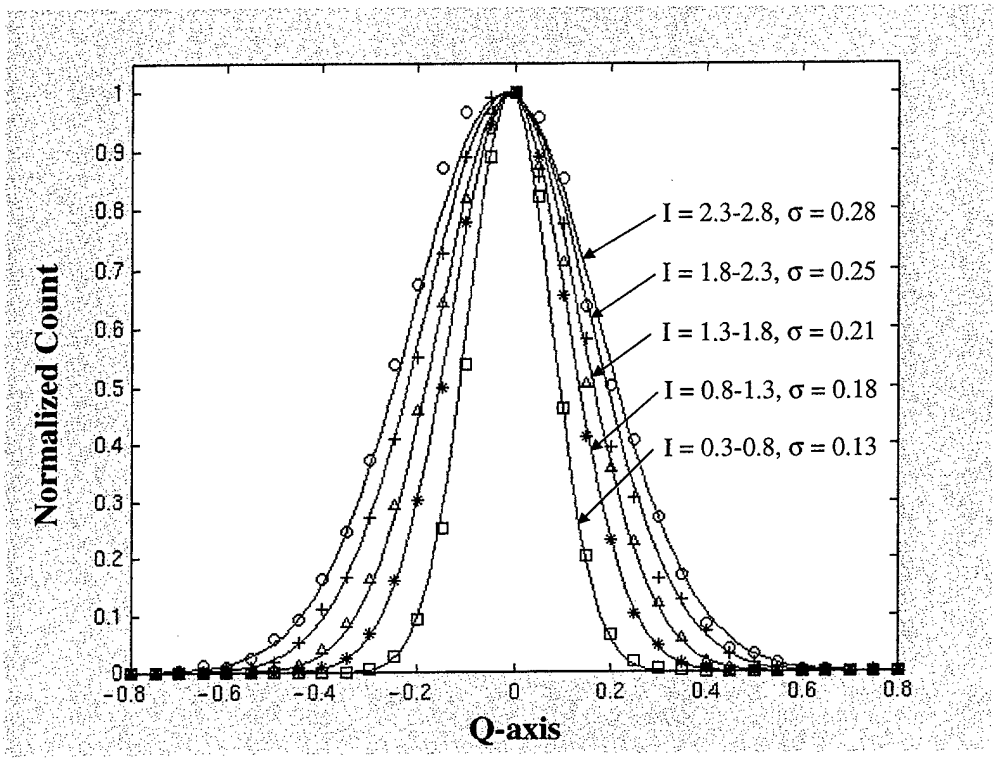

Fig. 10 Q-component distributions at different I-component range intervals.

Proceeding with the curving fitting, one obtains a best-fit curve "$10 \cdot |y|^{4.2} - 0.2$" as the detector for target extraction (see Fig. 9). Passing the SAR/ATI signal through this detector, one obtains a MTI plot as shown in Fig. 11. Similar to the SAR/DPCA case, almost all of the 15 m/s and 10 m/s targets are detected except for the 20 m^2 RCS target #17. All the 3 m/s targets are missed except for target #8 and only two of the five 5 m/s targets are detected. All of the 20 m^2 RCS targets are missed except for target #18, suggesting that detection is noise-limited.

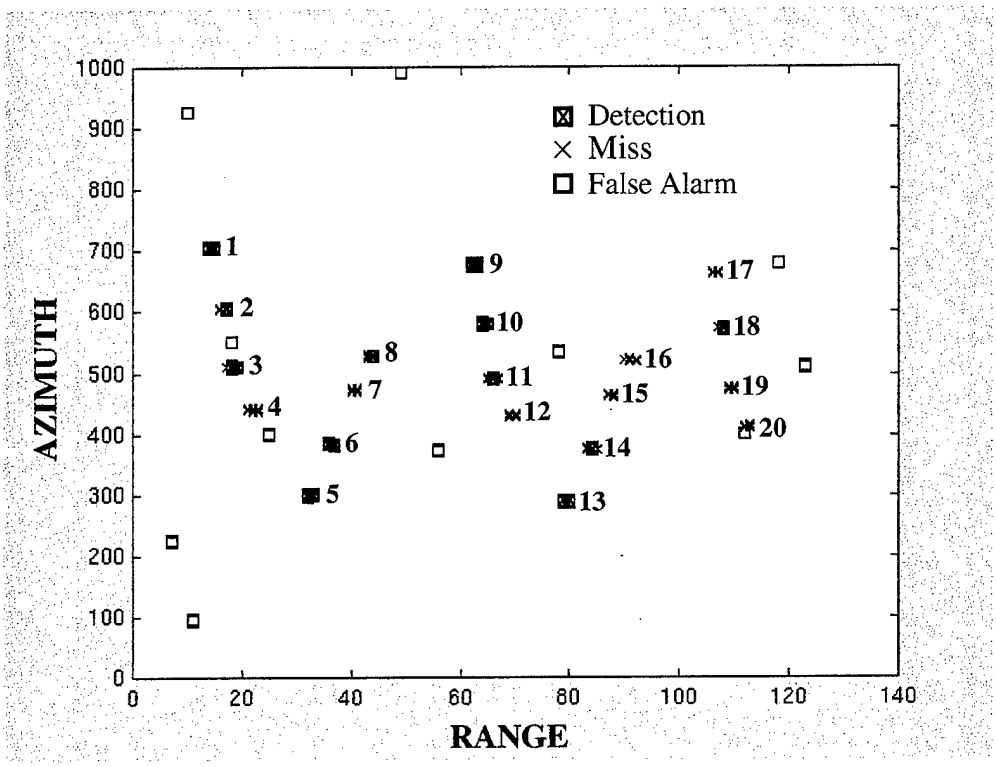

Fig. 11 Output of "$10 \cdot |y|^{4.2} - 0.2$" detector

In order to further validate the above results, four more simulation runs with exactly the same scenario but with different random number generation seeds are carried out. The results, including the ones just presented, are summarized in Table 3. The results from the four additional runs are consistent with the previous result, further indicating that the two processing approaches are similar in their GMTI performances. The SAR/ DPCA has an average of 12.6 detections and 7.0 false alarms. On the other hand, the SAR/ATI has a slightly lower average detection value of 12.4 with a slightly higher number of false alarms of 7.8. Given the relatively small number of runs, this small difference is not statistically significant, and one could safely conclude that the two processor performances are essentially the same using the R2 Standard Beam Mode.

Table 3: Comparison of SAR/DPCA and SAR/ATI Processors

Simulation Run Filename	**SAR/DPCA**		**SAR/ATI**	
	Detection	**False Alarms**	**Detection**	**False Alarms**
r2_w3_s2000_6_e	12	10	13	10
Jul25_00#1	14	9	12	10
Jul25_00#2	11	1	13	1
Jul25_00#4	13	4	10	5
Jul25_00#5	13	11	14	13
Average	**12.6 ± 1.2**	**7.0 ± 4.3**	**12.4 ± 1.5**	**7.8 ± 4.8**

7.0 Comparison of Processors

At first, SAR/ATI would appear to have an advantage over SAR/DPCA in that the ideal PRF is no longer required. The two-antenna SAR/DPCA suffers the shortcoming of any two-pulse delay-line canceller in that its output signal is equal to the difference of two slightly different signal vectors and its magnitude is related to the target radial velocity as follows:

$$a = |\mathbf{S}_1 - \mathbf{S}_2| = |S(x,y)|\left|1 - e^{j4\pi(R_2 - R_1)/\lambda}\right|$$

which simplifies to:

$$a = 2 \cdot \left|\sin\left(\frac{2\pi(R_2 - R_1)}{\lambda}\right)\right| \cdot |S(x,y)|$$
$$= 2 \cdot \left|\sin\left(2\pi\frac{V_r \delta t}{\lambda}\right)\right| \cdot |S(x,y)| \quad ,$$

where R_1 and R_2 are ranges from the forward and aftward phase centers, respectively, to the moving target, and V_r is the target radial velocity. δt is the "DPCA time," which in this case is equal to the pulse repetition interval (PRI). Thus, slow-moving targets are significantly attenuated by the DPCA clutter rejection filter.

On the other hand, the SAR/ATI output is the signal power (as opposed to the signal voltage from the SAR/DPCA processor) and its magnitude is simply equal to $|S(x,y)|^2$. The targets are not suppressed along with the stationary clutter when one utilizes phase and amplitude information for target extraction. Careful examination of the SAR/ATI processor shows that the SAR/ATI phase depends on the signal-to-clutter ratio (SCR). For example, in a 25 m × 25 m resolution cell, target and clutter signal vectors will be added within the cell. Ignoring thermal noise, the output image from the first channel can be written as

$$S_1 = V_{s,1} + V_c \,,$$

where V_c is the clutter and $V_{s,1}$ is the signal from the target of interest in channel 1. Similarly, for channel 2 we can write

$$S_2 = V_{s,2} + V_c \,.$$

The estimated phase from the SAR/ATI processor output is

$$\text{Arctan}(S_1 \cdot S_2^*) \,.$$

But the correct interferometric phase for the signal of interest is

$$\text{Arctan}(V_{s,1} \cdot V_{s,2}^{*}) .$$

Therefore, the estimated phase is "attenuated" by the clutter contained in the same resolution cell as the target. The smaller the SCR, the more likely the target will become buried within the main clutter region in the complex plane and less likely be extracted from the clutter. As illustrated in Fig. 12, the resulting signal vector within a resolution cell has a phase angle that is consistently smaller than the actual moving target's signal phase. For a clutter vector that is the same magnitude as the target vector, the resulting signal vector would have a phase value that is exactly half of that of the moving target. The effect will be most severe for small SCR targets. This is indeed observed for targets 17 to 20, where only target 18 has a confirmed detection. However, the clutter contamination effect may be mitigated by selecting radar resolution cell areas that are comparable in physical size to that of the target so that the clutter contribution is small with respect to the target signal. For RADARSAT2 MODEX studies, cell sizes of 6 m × 6 m and smaller may be needed to extract weak targets.

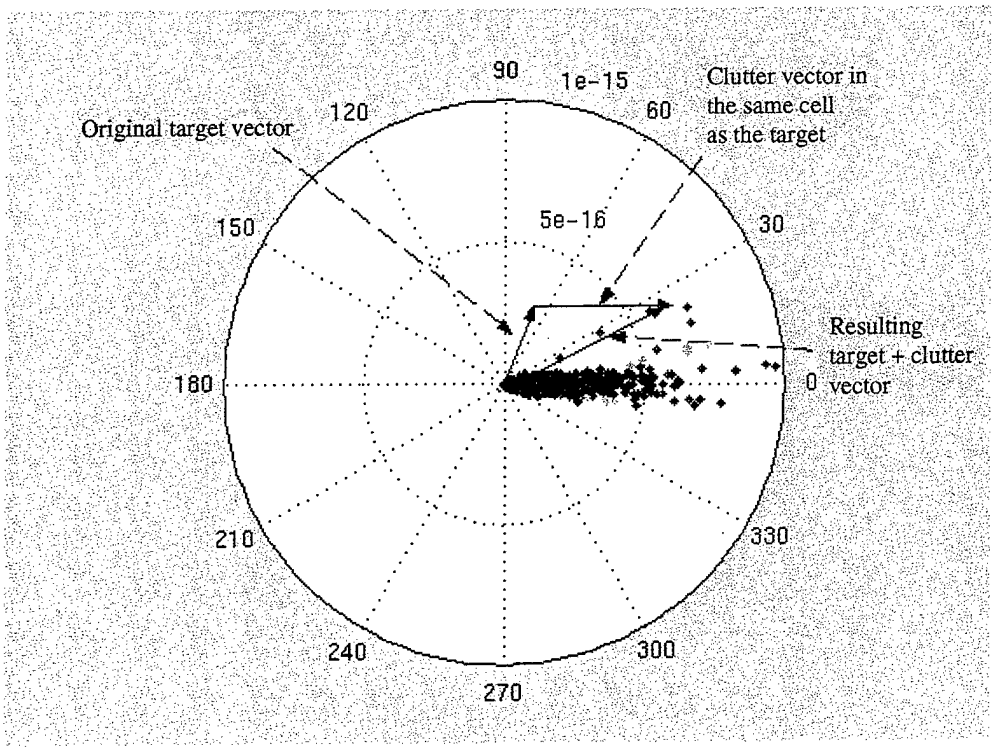

Fig. 12 Target signal phase within a resolution cell is being "attenuated" with the clutter signal occupying the same cell.

In SAR/ATI processing, noise tends to scatter the clutter signal around zero phase and may obscure nearby targets with small phase angles. High system noise could potentially present a problem for detecting bright but slow moving targets. However, the overall performance of the SAR/ATI processor was shown to be about the same as that of the SAR/DPCA approach for the target and clutter parameters examined.

On the other hand, both SAR/ATI and SAR/DPCA suffer from the limited efficiency of the two-pulse canceller. To get high sensitivity, the two antennas have to be widely separated, but this leads to a comb of blind velocities $v_{blind} = kv_p\lambda/d$, where k is an integer, v_p is the platform velocity, and d is the antenna separation.

8.0 Target Signal Contamination by Background Clutter

As discussed earlier, due to SAR's finite resolution cell sizes (25m × 25m for R2), clutter signals within the cell containing a moving target are added to the target's signal vectorially. Therefore, the phase of the moving target is reduced by the clutter signal vector which lies along the zero-phase line in the complex plane. The overall effect of the clutter contamination would be reduced if the target's physical size is comparable to the area of the resolution cell, that is, the clutter contribution within the cell containing a moving target is small compared to the target contribution. The question is how much of the clutter contribution is coming from the target's true location and how much is coming from its shifted position. In the following investigation, one would like to examine the clutter contributions from both the target's true position and its azimuthally-shifted location.

8.1 Clutter Contamination:

There are two possible sources of clutter contamination — one from the clutter signal of the target's shifted position and the other from that of the target's original location. The latter component of the contamination can be minimized if the target's physical size is close to the area of the resolution cell, but the contribution from the clutter at the shifted position cannot be avoid. Due to the matched filter processing, however, the clutter contamination from the moving target's pre-shifted or true position is expected to be much smaller than that of the shifted location, as illustrated Fig. 13. As can be seen from the figure, the matched filter for the stationary terrain captures most of the energy of stationary objects but only a negligible amount of the energy of the moving target at its pre-shifted position. This is expected since the filter is "matched" to the stationary objects only. As the matched filter centered at zero-Doppler slides along the slow-time axis, it captures part of the energy of the moving target at either an earlier or later instant in the slow-time axis (i.e., at its shifted azimuth location) depending on the direction of the target's radial velocity. This partially captured energy of the moving target is added vectorially to the fully-captured energy of the terrain at its shifted location as depicted in the figure. Thus, the moving target's energy is contaminated mostly by the clutter energy from the target's shifted position. One verifies this experimentally using a set of carefully designed target-clutter scenarios in the next sub-section.

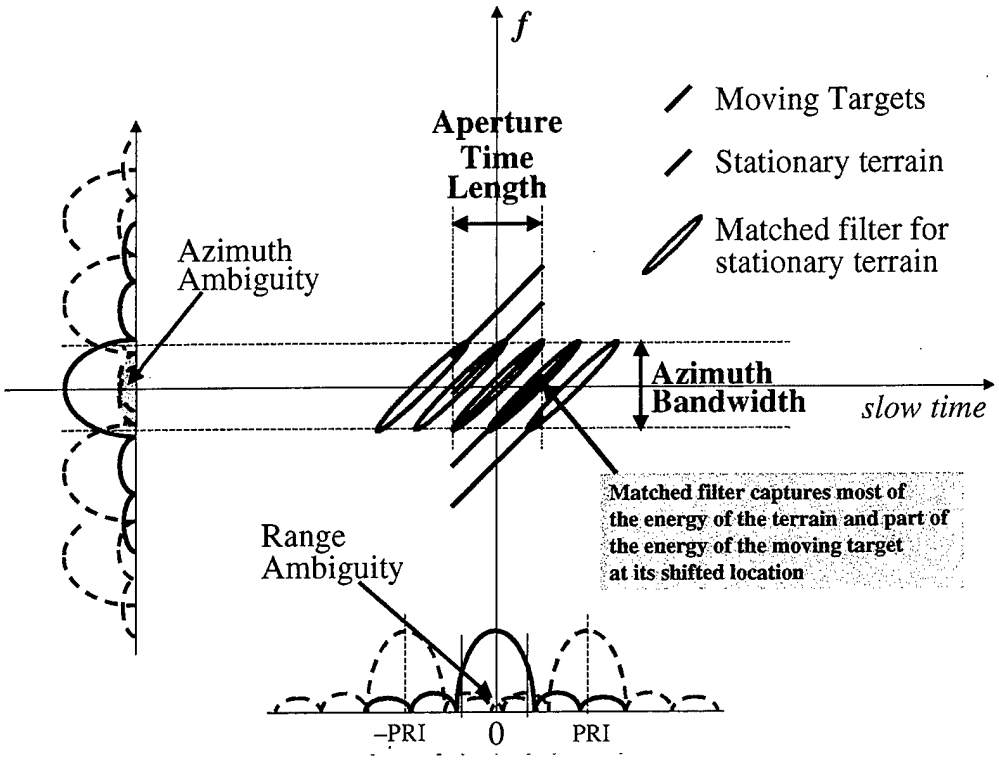

Fig. 13 Illustrations of a matched filter for stationary terrain, and noise-like contributions due to range and azimuth ambiguities.

8.2 Simulation Results:

Four moving targets with varying speeds are placed beside a land patch as shown in the corner insert of Fig. 14. The detailed simulation parameters are listed in Appendix B.

The targets are initially situated in a clutterless region and are moving westward in such a way that after the SAR processing their shifted positions are also situated outside the clutter patch (see Fig. 14). This will ensure that the target's signal has no clutter contamination coming from both the target's true position and its shifted position. The target's phase and amplitude are expected to be derived purely from its velocity and reflectivity. The radar raw signal is generated for the RADARSAT 2 standard beam mode. The system thermal noise is set to zero so that only the targets and the clutter are present in the scene.

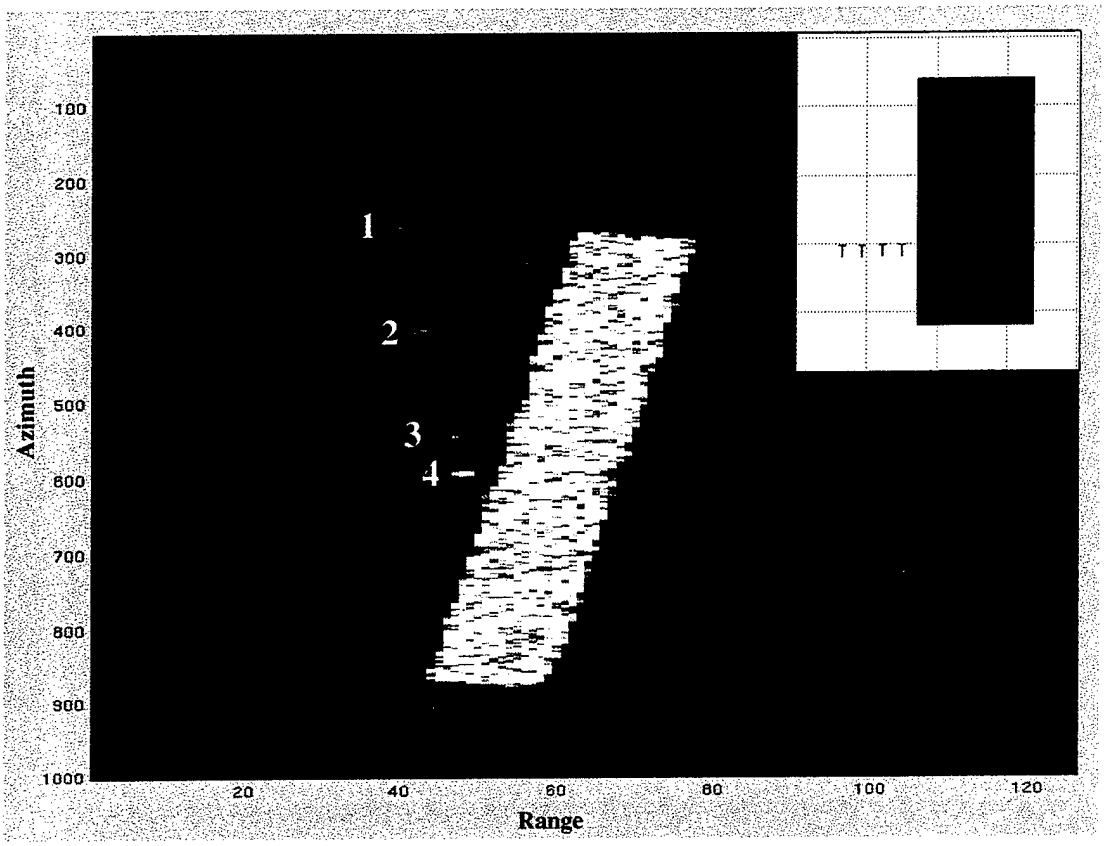

Fig. 14 ATI processor output: stationary clutter (white), moving targets (red)

As can be seen from Fig. 15, the SAR/ATI processed signals of the moving targets are very "clean" with very little scatter or spread, resulting from the clutter contamination and the system noise. This ideal case serves as the reference baseline with which all other cases may be compared.

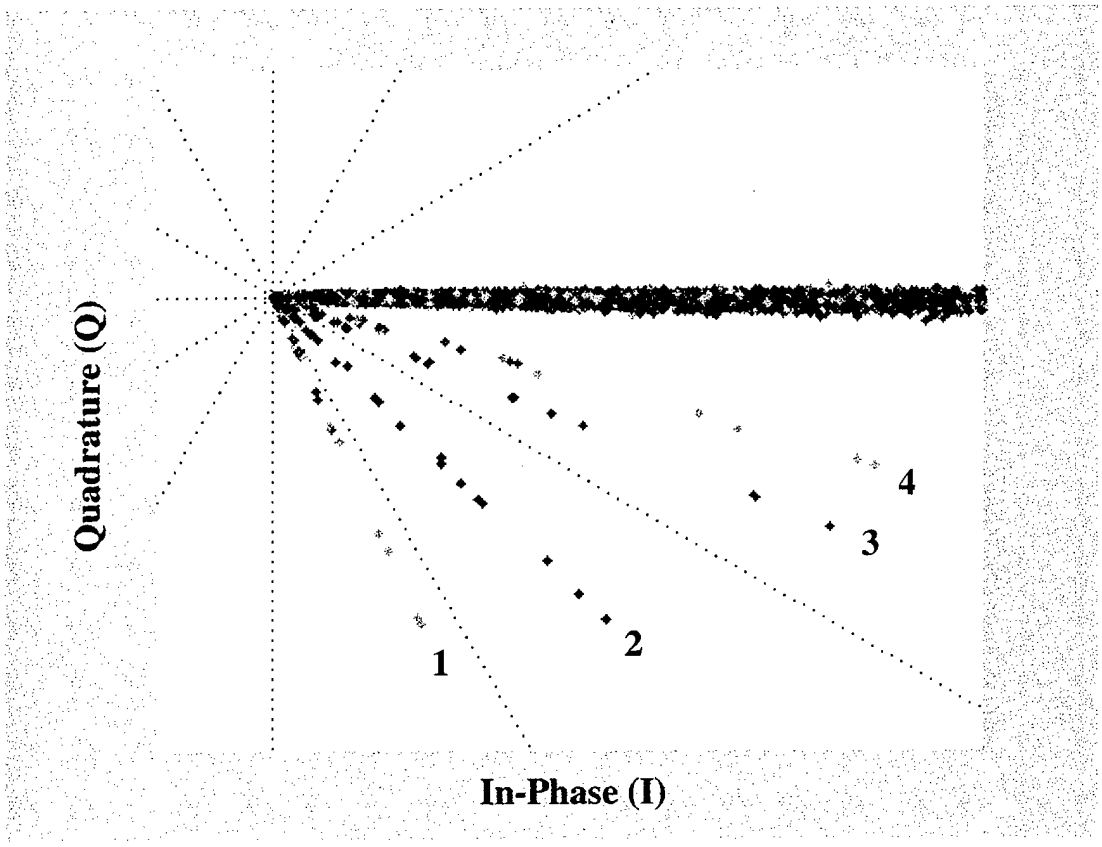

Fig. 15 Phase-amplitude plot of the SAR/ATI processed signal

Next we place the same moving targets inside the land patch as shown in the corner insert of Fig. 16. The targets are purposely placed near the edge of the land patch so that the SAR processing will shift them outside the patch as can be seen in Fig. 16. Since the shifted position has no clutter and the system thermal noise is set to zero, the only possible source of target signal contamination must come from its pre-shifted location, which contains the land clutter. This will test whether or not the clutter from the target's pre-shifted position contributes significantly to the target's apparent signal phase and amplitude. Fig. 17 plots the SAR/ATI processed signals in a complex plane showing targets' phases and amplitudes. Comparing this result with that of the reference case, one notes that there is essentially no difference between the two, confirming our previous expectation that the clutter contamination from the moving target's pre-shifted position is negligibly small.

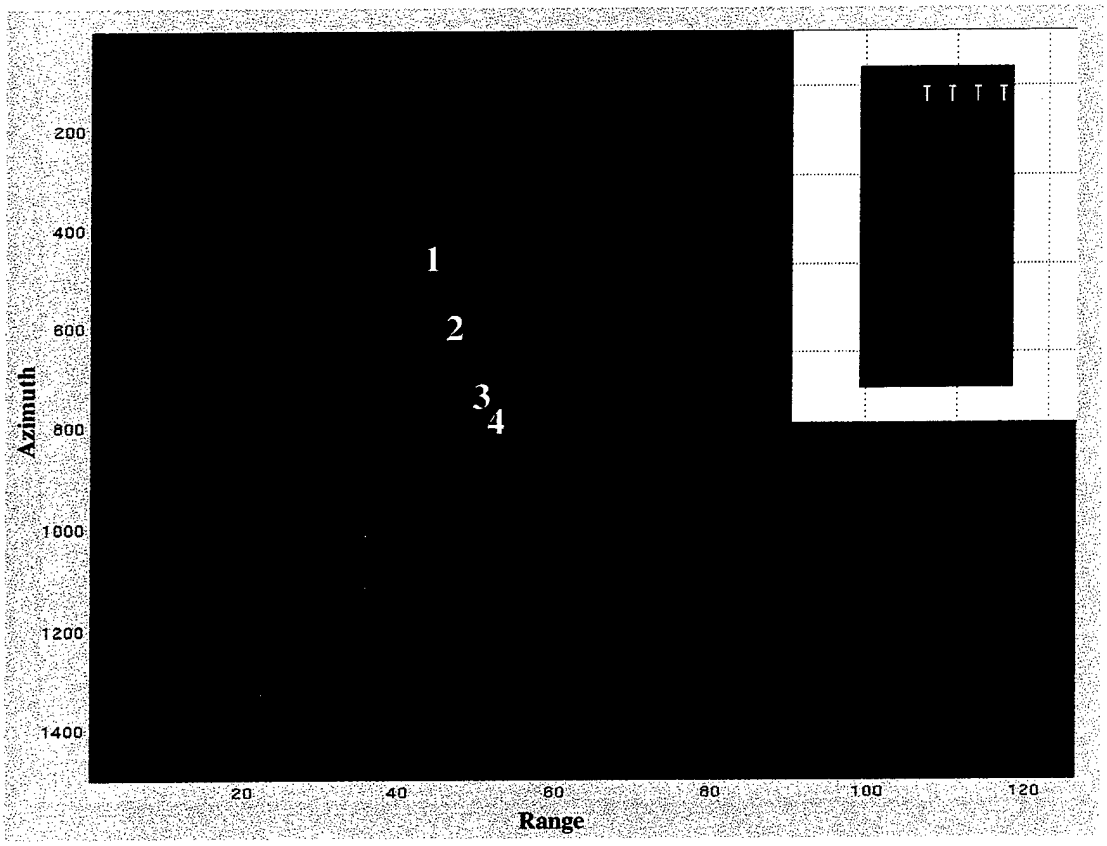

Fig. 16 Moving targets are placed, initially, inside the land patch but are shifted outside the patch after SAR processing

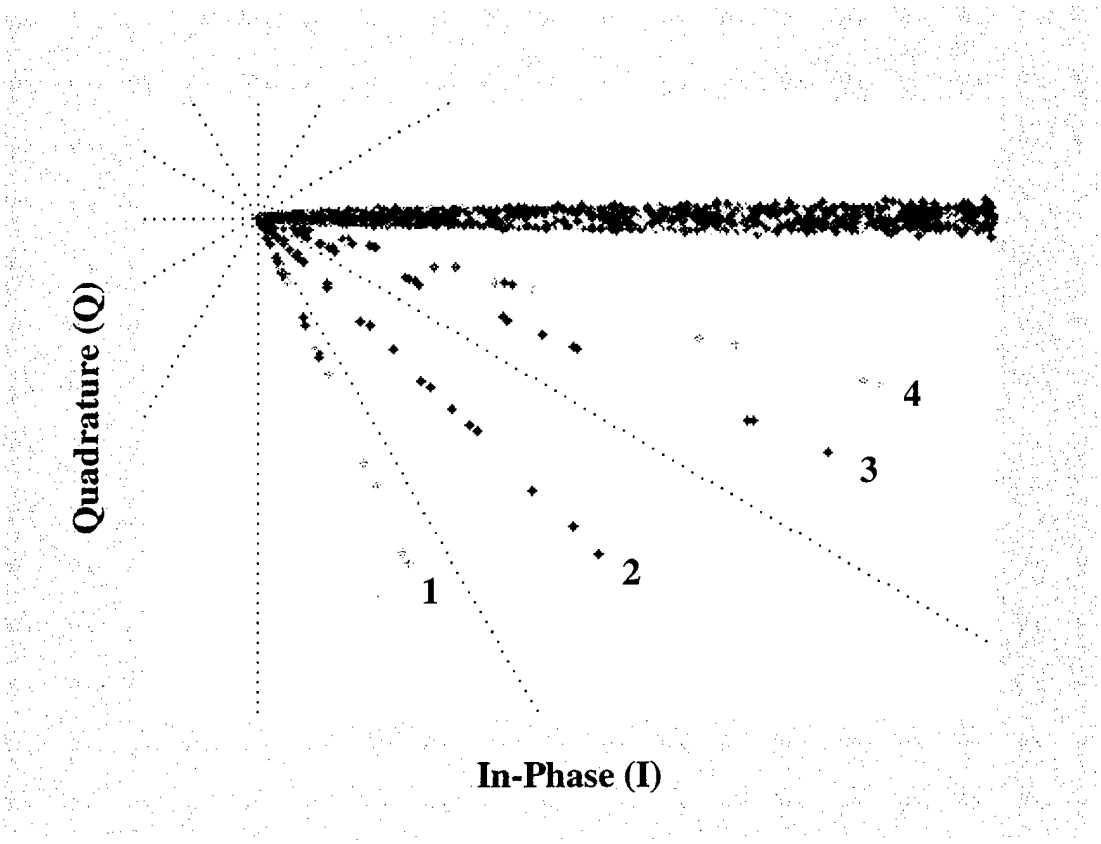

Fig. 17 Amplitude-phase plot of SAR/ATI processed signal from four moving targets initially placed inside a clutter patch

Our next simulation involves placing the same moving targets initially in a clutterless region but near a land patch so that their SAR processed positions fall inside the clutter patch region as depicted in Fig. 18.

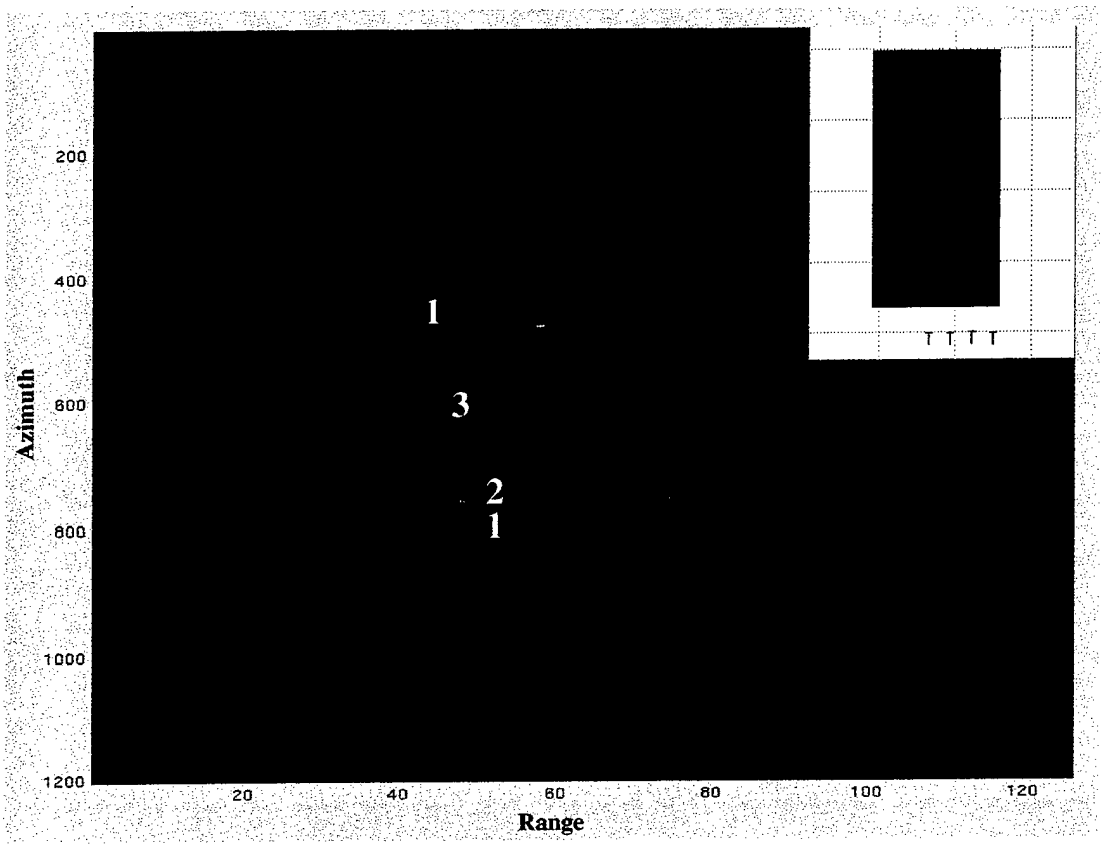

Fig. 18 Moving targets are placed initially outside but near a land patch. Three of the four targets are shifted inside the clutter patch after SAR processing

This experiment would provide the degree of target signal contamination by the clutter coming from the shifted position. The SAR/ATI complex signal output, as shown in Fig. 19, clearly indicates visible changes in the processed signal compared to that of the baseline.

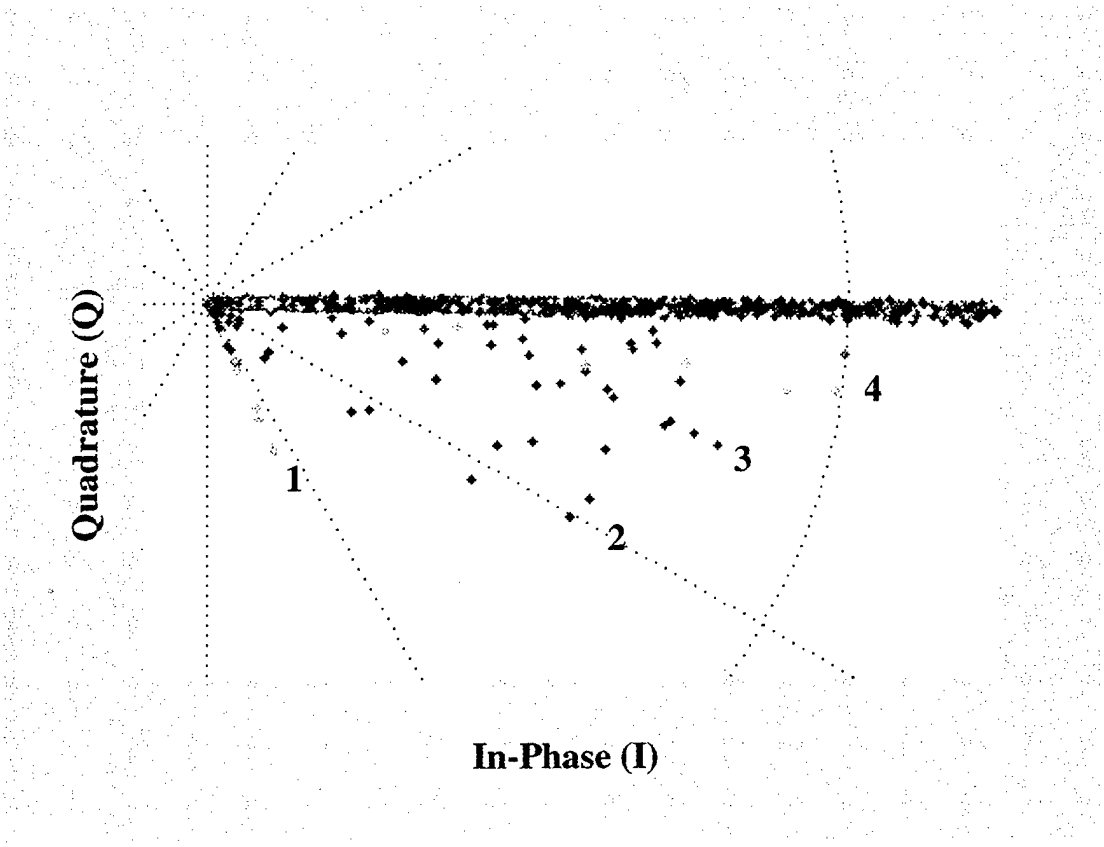

Fig. 19 Amplitude-phase plot of SAR/ATI processed signal from four moving targets initially placed outside a clutter patch but shifted inside the patch by SAR processing

The three targets that are shifted inside the clutter patch show clear signs of clutter contamination manifested by reduced phase angles and with more scatter in the signal phases. The apparent amplitudes of these targets have also increased due to the clutter signal contribution. As expected, the target that is shifted outside the patch shows no sign of signal contamination.

The present result clearly shows that the clutter contamination from the moving target's pre-shifted position is negligible and that the contamination comes mainly from the SAR-shifted position. The matched filter processing is shown to be very effective in filtering out the moving targets from the stationary terrain.

9.0 Conclusions

At the onset of the study, it was expected that SAR/ATI would outperform classical SAR/DPCA when the SCR is high and that SAR/DPCA would be superior when the SCR is low. But this expectation does not appear to be supported by the present study. The two processor architectures both appear to perform well under the target and clutter parameters examined. Both approaches are capable of detecting targets with radial speed above 5 m/s and RCS larger than 20 m^2. The initial simulation results here are encouraging, and suggest that detection of ground moving targets of sufficient radar cross section is possible with a sensor of the RADARSAT2 GMTI class. Further studies are expected to refine these performance data and to characterize the full range of a space-based GMTI capability.

References

[1] Coe, D.J., White, R.G., " Moving Target Detection in SAR Imagery: Experimental Results," IEEE International Radar Conference, 1995, 644-649.

[2] Stockburger, E.F., Held, D.N., "Interferometric Moving Ground Target Imaging," IEEE International Radar Conference, 1995, 438-443.

[3] Ender, J.H.G., "Space-Time Processing for Multichannel Synthetic Aperture Radar," Electronics & Communication Engineering Journal, 11, 1999, 29-38.

[4] Yadin, E., "Evaluation of Noise and Clutter Induced Relocation Error in SAR MTI," IEEE International Radar Conference, 1995, 650-655.

[5] Livingstone, C., "The Addition of MTI Modes to Commercial SAR Satellites," Proc. Of 10th CASI Conference on Astronautics, Ottawa, Canada, October 26-28, 1998.

[6] Luscombe, A., "The Radarsat Project," IEEE Canadian Review, Fall 1995.

Appendix A: Signal Generation Parameters

Filename: r2_w3_s2000_6_e
Platform: SBR
Orbit: altitude (km) 792, inclination (deg) 98.6
Initial sub satellite point: longitude (deg) -90, latitude (deg) 47
Initial SBR direction: NORTH
peak power (watts): 5120
carrier frequency (GHz): 5.4
expanded pulse width (usec): 42
pulse bandwidth (MHz): 11.58
burst length (sec): 0.75
noise temperature (K): 1893
prf (Hz): 1988.3
A/D sampling rate (MHz): 12.66
waveform modulation: LFM
model receiver: yes
IF bandwidth (MHz): 12
IF filter type: Butterworth
IF filter order: 8
IF centre frequency (MHz): 1500
channel to channel mismatch (dB): -50
A/D quantization level (dB): -110
number of A/D bits: 8
number of Mismatch Ripples: 4
PRI compensation: no
ZRT compensation: no
radar system loss (dB): 0
spotlighting: no
fill pulse duration (ms): 0
model phase noise: no

thermal noise seed: 123456789
antenna seed: 232323232
clutter seed: 777777777
target seed: 567567567
jammer seed: 372372372
motion seed: 952952952
channel response seed: 101001000
available memory (MB): 200
brute-force pulse summation: no
pulse oversampling factor: 11
brute-force antenna patterns: no
pattern oversampling factor: 30

array type: phased_array
number of receive apertures: 2
grid spacing along x (m): 0.046
grid spacing along y (m): 0.046
random sidelobe level (dB): -50
physical shape: rectangular

```
TRANSMIT APERTURE:
x-width (m): 15
y-width (m): 0.75
x position (m): 0
y position (m): 0
x taper: uniform
y taper: uniform

RECEIVE APERTURE 1:
x-width (m): 7.5
y-width (m): 0.75
x position (m): -3.75
y position (m): 0
x taper: uniform
y taper: taylor
y sidelobe level (dB): -40

RECEIVE APERTURE 2:
x-width (m): 7.5
y-width (m): 0.75
x position (m): 3.75
y position (m): 0
x taper: uniform
y taper: taylor
y sidelobe level (dB): -40

SWATH longitude: -81.8249
swath latitude: 48.1904
swath range width (m): 1500

MECH BORESIGHT longitude: -81.8249
mech boresight latitude: 48.1904
mech boresight frd azimuth: 87.481
mech boresight elevation: 37.2849

ELEC BORESIGHT longitude: -81.8249
elec boresight latitude: 48.1904
elec boresight frd azimuth: 87.481
elec boresight elevation: 37.2849

TARGET number: 20
type: Wheeled
longitude (deg): -81.8207
latitude (deg): 48.2218
backscatter statistics: fixed
mean target RCS (m^2): 20
speed (km/h): 12
heading East of North (deg): 90
spectral width (m/s): 0

TARGET number: 19
type: Wheeled
longitude (deg): -81.8213
latitude (deg): 48.2212
```

```
backscatter statistics: fixed
mean target RCS (m^2): 20
speed (km/h): 18
heading East of North (deg): 90
spectral width (m/s): 0

TARGET number: 18
type: Wheeled
longitude (deg): -81.822
latitude (deg): 48.2223
backscatter statistics: fixed
mean target RCS (m^2): 20
speed (km/h): 36
heading East of North (deg): 90
spectral width (m/s): 0

TARGET number: 17
type: Wheeled
longitude (deg): -81.8227
latitude (deg): 48.2237
backscatter statistics: fixed
mean target RCS (m^2): 20
speed (km/h): 54
heading East of North (deg): 90
spectral width (m/s): 0

TARGET number: 16
type: Wheeled
longitude (deg): -81.8235
latitude (deg): 48.2126
backscatter statistics: fixed
mean target RCS (m^2): 30
speed (km/h): 12
heading East of North (deg): -90
spectral width (m/s): 0

TARGET number: 15
type: Wheeled
longitude (deg): -81.8244
latitude (deg): 48.2128
backscatter statistics: fixed
mean target RCS (m^2): 30
speed (km/h): 18
heading East of North (deg): -90
spectral width (m/s): 0

TARGET number: 14
type: Wheeled
longitude (deg): -81.8249
latitude (deg): 48.2112
backscatter statistics: fixed
mean target RCS (m^2): 30
speed (km/h): 36
heading East of North (deg): -90
```

```
spectral width (m/s): 0

TARGET number: 13
type: Wheeled
longitude (deg): -81.8255
latitude (deg): 48.2095
backscatter statistics: fixed
mean target RCS (m^2): 30
speed (km/h): 54
heading East of North (deg): -90
spectral width (m/s): 0

TARGET number: 12
type: Wheeled
longitude (deg): -81.8306
latitude (deg): 48.2201
backscatter statistics: fixed
mean target RCS (m^2): 35
speed (km/h): 12
heading East of North (deg): 90
spectral width (m/s): 0

TARGET number: 11
type: Wheeled
longitude (deg): -81.8313
latitude (deg): 48.2196
backscatter statistics: fixed
mean target RCS (m^2): 35
speed (km/h): 18
heading East of North (deg): 90
spectral width (m/s): 0

TARGET number: 10
type: Wheeled
longitude (deg): -81.832
latitude (deg): 48.221
backscatter statistics: fixed
mean target RCS (m^2): 35
speed (km/h): 36
heading East of North (deg): 90
spectral width (m/s): 0

TARGET number: 9
type: Wheeled
longitude (deg): -81.8327
latitude (deg): 48.2222
backscatter statistics: fixed
mean target RCS (m^2): 35
speed (km/h): 54
heading East of North (deg): 90
spectral width (m/s): 0

TARGET number: 8
type: Wheeled
```

```
longitude (deg): -81.8345
latitude (deg): 48.2112
backscatter statistics: fixed
mean target RCS (m^2): 40
speed (km/h): 12
heading East of North (deg): -90
spectral width (m/s): 0

TARGET number: 7
type: Wheeled
longitude (deg): -81.8353
latitude (deg): 48.2114
backscatter statistics: fixed
mean target RCS (m^2): 40
speed (km/h): 18
heading East of North (deg): -90
spectral width (m/s): 0

TARGET number: 6
type: Wheeled
longitude (deg): -81.8358
latitude (deg): 48.2098
backscatter statistics: fixed
mean target RCS (m^2): 40
speed (km/h): 36
heading East of North (deg): -90
spectral width (m/s): 0

TARGET number: 5
type: Wheeled
longitude (deg): -81.8364
latitude (deg): 48.2081
backscatter statistics: fixed
mean target RCS (m^2): 40
speed (km/h): 54
heading East of North (deg): -90
spectral width (m/s): 0

TARGET number: 4
type: Wheeled
longitude (deg): -81.8415
latitude (deg): 48.2187
backscatter statistics: fixed
mean target RCS (m^2): 45
speed (km/h): 12
heading East of North (deg): 90
spectral width (m/s): 0

TARGET number: 3
type: Wheeled
longitude (deg): -81.8422
latitude (deg): 48.2179
backscatter statistics: fixed
mean target RCS (m^2): 45
```

```
speed (km/h): 18
heading East of North (deg): 90
spectral width (m/s): 0

TARGET number: 2
type: Wheeled
longitude (deg): -81.8429
latitude (deg): 48.2191
backscatter statistics: fixed
mean target RCS (m^2): 45
speed (km/h): 36
heading East of North (deg): 90
spectral width (m/s): 0

TARGET number: 1
type: Wheeled
longitude (deg): -81.8436
latitude (deg): 48.2202
backscatter statistics: fixed
mean target RCS (m^2): 45
speed (km/h): 54
heading East of North (deg): 90
spectral width (m/s): 0

PATCH number: 1
type: land
centre longitude (deg): -81.8324
centre latitude (deg): 48.2178
long-size (km): 2.5
lat-size (km): 5
along-range scatterer spacing (m): 10
cross-range scatterer spacing (m): 4
backscatter statistics: rayleigh
mean clutter cross-section (m^2/m^2): 0.1
spectral width (m/s): 0.1
```

Appendix B: Signal Generation Parameters

Filename: Sep01_00#4
Platform: SBR
Orbit: altitude (km) 792, inclination (deg) 98.6
Initial sub satellite point: longitude (deg) -90, latitude (deg) 47
Initial SBR direction: NORTH
peak power (watts): 5120
carrier frequency (GHz): 5.4
expanded pulse width (usec): 42
pulse bandwidth (MHz): 11.58
burst length (sec): 0.75
noise temperature (K): 1
prf (Hz): 1988.3
A/D sampling rate (MHz): 12.66
waveform modulation: LFM
model receiver: yes
IF bandwidth (MHz): 12
IF filter type: Butterworth
IF filter order: 8
IF centre frequency (MHz): 1500
channel to channel mismatch (dB): -50
A/D quantization level (dB): -110
number of A/D bits: 8
number of Mismatch Ripples: 4
PRI compensation: no
ZRT compensation: no
radar system loss (dB): 0
spotlighting: no
fill pulse duration (ms): 0
model phase noise: no

thermal noise seed: 123456789
antenna seed: 232323232
clutter seed: 777777777
target seed: 567567567
jammer seed: 372372372
motion seed: 952952952
channel response seed: 101001000
available memory (MB): 600
brute-force pulse summation: no
pulse oversampling factor: 11
brute-force antenna patterns: no
pattern oversampling factor: 30

array type: phased_array
number of receive apertures: 2
grid spacing along x (m): 0.046
grid spacing along y (m): 0.046
random sidelobe level (dB): -50
physical shape: rectangular

```
TRANSMIT APERTURE:
x-width (m): 15
y-width (m): 0.75
x position (m): 0
y position (m): 0
x taper: uniform
y taper: uniform

RECEIVE APERTURE 1:
x-width (m): 7.5
y-width (m): 0.75
x position (m): -3.75
y position (m): 0
x taper: uniform
y taper: taylor
y sidelobe level (dB): -40

RECEIVE APERTURE 2:
x-width (m): 7.5
y-width (m): 0.75
x position (m): 3.75
y position (m): 0
x taper: uniform
y taper: taylor
y sidelobe level (dB): -40

SWATH longitude: -81.8249
swath latitude: 48.1904
swath range width (m): 1500

MECH BORESIGHT longitude: -81.8249
mech boresight latitude: 48.1904
mech boresight frd azimuth: 87.481
mech boresight elevation: 37.2849

ELEC BORESIGHT longitude: -81.8249
elec boresight latitude: 48.1904
elec boresight frd azimuth: 87.481
elec boresight elevation: 37.2849

TARGET number: 1
type: Wheeled
longitude (deg): -81.833
latitude (deg): 48.2094
backscatter statistics: fixed
mean target RCS (m^2): 40
speed (km/h): 12
heading East of North (deg): -90
spectral width (m/s): 0

TARGET number: 2
type: Wheeled
longitude (deg): -81.8336
latitude (deg): 48.2094
```

```
backscatter statistics: fixed
mean target RCS (m^2): 40
speed (km/h): 18
heading East of North (deg): -90
spectral width (m/s): 0

TARGET number: 3
type: Wheeled
longitude (deg): -81.8341
latitude (deg): 48.2094
backscatter statistics: fixed
mean target RCS (m^2): 40
speed (km/h): 36
heading East of North (deg): -90
spectral width (m/s): 0

TARGET number: 4
type: Wheeled
longitude (deg): -81.8347
latitude (deg): 48.2094
backscatter statistics: fixed
mean target RCS (m^2): 40
speed (km/h): 54
heading East of North (deg): -90
spectral width (m/s): 0

PATCH number: 1
type: land
centre longitude (deg): -81.8309
centre latitude (deg): 48.213
long-size (km): 0.245
lat-size (km): 2
along-range scatterer spacing (m): 2
cross-range scatterer spacing (m): 2
backscatter statistics: rayleigh
mean clutter cross-section (m^2/m^2): 0.1
spectral width (m/s): 0.1
```

List of symbols/abbreviations/acronyms/initialisms

ATI	Along-Track Interferometry
CFAR	Constant False Alarm Rate
DND	Department of National Defence
DPCA	Displaced Phase Center Antenna
DREO	Defence Research Establishment Ottawa
GMTI	Ground Moving Target Indication
I-Q	In-Phase & Quadrature
MODEX	Moving Object Detection Experiment
P_{FA}	Probability of False Alarm
PRF	Pulse Repetition Frequency
PRI	Pulse Repetition Interval
R2	RADARSAT2
RCS	Radar Cross Section
SAR	Synthetic Aperture Radar
SBR	Space-Based Radar
SCR	Signal-to-Clutter Ratio
STAP	Space-Time Adaptive Processing

UNCLASSIFIED
SECURITY CLASSIFICATION OF FORM
(highest classification of Title, Abstract, Keywords)

DOCUMENT CONTROL DATA

(Security classification of title, body of abstract and indexing annotation must be entered when the overall document is classified)

1. ORIGINATOR (the name and address of the organization preparing the document. Organizations for whom the document was prepared, e.g. Establishment sponsoring a contractor's report, or tasking agency, are entered in section 8.)

Defence Research Establishment Ottawa
3701 Carling Avenue
Ottawa, Ontario, Canada K1A 0Z4

2. SECURITY CLASSIFICATION (overall security classification of the document, including special warning terms if applicable)

UNCLASSIFIED

3. TITLE (the complete document title as indicated on the title page. Its classification should be indicated by the appropriate abbreviation (S,C or U) in parentheses after the title.)

An Analysis of RADARSAT2 SAR-GMTI Performance for Standard Beam Mode (U)

4. AUTHORS (Last name, first name, middle initial)

Chiu, Shen

5. DATE OF PUBLICATION (month and year of publication of document)	6a. NO. OF PAGES (total containing information. Include Annexes, Appendices, etc.)	6b. NO. OF REFS (total cited in document)
December 2000	40	6

7. DESCRIPTIVE NOTES (the category of the document, e.g. technical report, technical note or memorandum. If appropriate, enter the type of report, e.g. interim, progress, summary, annual or final. Give the inclusive dates when a specific reporting period is covered.)

DREO Technical Report

8. SPONSORING ACTIVITY (the name of the department project office or laboratory sponsoring the research and development. Include the address.)

Space Systems and Technology Section, Defence Research Establishment Ottawa
3701 Carling Avenue
Ottawa, Ontario, Canada K1A 0Z4

9a. PROJECT OR GRANT NO. (if appropriate, the applicable research and development project or grant number under which the document was written. Please specify whether project or grant)	9b. CONTRACT NO. (if appropriate, the applicable number under which the document was written)
5EG11	

10a. ORIGINATOR'S DOCUMENT NUMBER (the official document number by which the document is identified by the originating activity. This number must be unique to this document.)	10b. OTHER DOCUMENT NOS. (Any other numbers which may be assigned this document either by the originator or by the sponsor)
DREO TR 2000- 088	

11. DOCUMENT AVAILABILITY (any limitations on further dissemination of the document, other than those imposed by security classification)

(x) Unlimited distribution
( ) Distribution limited to defence departments and defence contractors; further distribution only as approved
( ) Distribution limited to defence departments and Canadian defence contractors; further distribution only as approved
( ) Distribution limited to government departments and agencies; further distribution only as approved
( ) Distribution limited to defence departments; further distribution only as approved
( ) Other (please specify):

12. DOCUMENT ANNOUNCEMENT (any limitation to the bibliographic announcement of this document. This will normally correspond to the Document Availability (11). However, where further distribution (beyond the audience specified in 11) is possible, a wider announcement audience may be selected.)

UNCLASSIFIED
SECURITY CLASSIFICATION OF FORM

13. ABSTRACT (a brief and factual summary of the document. It may also appear elsewhere in the body of the document itself. It is highly desirable that the abstract of classified documents be unclassified. Each paragraph of the abstract shall begin with an indication of the security classification of the information in the paragraph (unless the document itself is unclassified) represented as (S), (C), or (U). It is not necessary to include here abstracts in both official languages unless the text is bilingual).

Canada's RADARSAT2 (R2) commercial SAR satellite will have an experimental operating mode that will allow ground moving target indication (GMTI) measurements to be made with received data. This mode is also called MODEX (Moving Object Detection Experiment). In the GMTI or MODEX mode of operation, the spacecraft's radar antenna is partitioned into two apertures that sequentially observe the scene of interest from the same points in space. Data is simultaneously and coherently received from both apertures and is down-linked in parallel channels for processing to extract moving target radial speeds in their SAR image context. This paper provides an analysis of SAR-GMTI performance at the R2 Standard Beam Mode based on computer modeling and simulations. Two SAR-MTI processing approaches are being explored. One utilizes the classical DPCA clutter cancellation technique to provide sub-clutter visibility for dim slowly moving targets. The other is based on the along-track (temporal) SAR interferometer technique, where amplitude and phase information of the slow-moving targets are exploited to allow their extraction from the dominant clutter background. Performances of the two approaches are compared. Effects of target signal contamination by background clutter is also examined. The results indicate that the two processing approaches are similar in their GMTI performance.

14. KEYWORDS, DESCRIPTORS or IDENTIFIERS (technically meaningful terms or short phrases that characterize a document and could be helpful in cataloguing the document. They should be selected so that no security classification is required. Identifiers such as equipment model designation, trade name, military project code name, geographic location may also be included. If possible keywords should be selected from a published thesaurus. e.g. Thesaurus of Engineering and Scientific Terms (TEST) and that thesaurus-identified. If it is not possible to select indexing terms which are Unclassified, the classification of each should be indicated as with the title.)

SAR, GMTI, ATI, DPCA
Synthetic aperture radar
Ground moving target indication
Along-track interferometry
Displaced phase center antenna